

Transmission and scarring in graphene quantum dots

Liang Huang¹, Ying-Cheng Lai^{1,2}, David K Ferry^{1,2,3},
Richard Akis^{1,3} and Stephen M Goodnick^{1,2,3}

¹ Department of Electrical Engineering, Arizona State University, Tempe, AZ 85287, USA

² Department of Physics, Arizona State University, Tempe, AZ 85287, USA

³ Center for Solid State Electronics Research, Arizona State University, Tempe, AZ 85287, USA

Received 23 October 2008, in final form 13 December 2008

Published 27 July 2009

Online at stacks.iop.org/JPhysCM/21/344203

Abstract

We study electronic transport in quantum-dot structures made of graphene. Focusing on the rectangular dot geometry and utilizing the non-equilibrium Green's function to calculate the transmission in the tight-binding framework, we find significant fluctuations in the transmission as a function of the electron energy. The fluctuations are correlated with the formation of quantum scarring states, or pointer states in the dot. Both enhancement and suppression of transmission have been observed. As the size of the quantum dot is increased, more scarring states can be formed, leading to stronger transmission or conductance fluctuations.

(Some figures in this article are in colour only in the electronic version)

1. Introduction

Graphene, a single, one-atom-thick sheet of carbon atoms arranged in a honeycomb lattice, is the two-dimensional building block for carbon materials of every other dimensionality. Due to its peculiar honeycomb lattice structure and the resulting sp^2 bonding, the transport bands arise from the p_z orbitals normal to the plane and have a linear energy-momentum relation: $E \sim |\Delta\mathbf{k}|$ [1, 2]. As a result, the quasi-particles are chiral, massless Dirac fermions having a 'speed of light' $v_F \approx 10^8 \text{ cm s}^{-1}$ [3]. Because of the nature of these bands, the densities of the quasi-particles can be controlled by external electric fields. It is then expected that graphene will have important applications in nanoelectronics, including both electronic field-effect devices and chemical sensors. Indeed, graphene p-n junctions have been realized experimentally [4–7], where electron density changes gradually between two limiting values as a function of position. Also, the response to perpendicular external electric fields allows one to build field-effect transistors (FETs) [8–10]. Experimental results from transport measurements show that graphene has a remarkably high electron mobility at room temperature, with reported values in excess of $120\,000 \text{ cm}^2 \text{ V}^{-1} \text{ s}^{-1}$ [11]. Graphene nanoribbons (GNRs) are thus potentially capable of supplementing conventional semiconductor materials in a wide range of nanotechnology [12, 13].

GNRs are especially useful, as these single layers are cut in a particular lateral pattern to yield certain electrical properties, including the opening of band-gaps due to this lateral confinement. Depending on how the outside edges are configured, say, zigzag or armchair, different properties emerge. Calculations based on the tight-binding method predict that zigzag GNRs are always metallic while armchair GNRs can be either metallic or semiconducting, depending on their exact width. While the metallic nature of zigzag GNRs is maintained by edge states, armchair GNRs, when semiconducting, have an energy gap scaling with the inverse of the GNR width [14]. Indeed, experimental results show that the energy gaps do increase with decreasing GNR width [15]. The high electrical and thermal conductivities of GNRs also make them a possible alternative to copper for integrated circuit interconnects. When a certain section of a GNR is designed to have a wider geometry from the rest of the GNR, a dot structure emerges, generating quantum confinement [16].

The complicated properties of graphene itself are only now beginning to be understood, and the detailed many-body physics has been shown to be important [17, 18]. Because of the high mobility and long coherence length, the details of many-body interactions and strong coherence over reasonable device sizes means that the simple quasi-classical approaches used in most semiconductors are not adequate in graphene. Instead, non-equilibrium Green's function (NEGF) formalism should be employed.

In this paper, we study electronic transport in graphene quantum dots. Because of the relativistic characteristics of electron motion in graphene, understanding the quantum transport properties is a problem not only of fundamental interest, but also of significant implications to device development. To be concrete, we shall focus on a particular class of dots, structures having a rectangular geometry. The basic quantity characterizing quantum transport is conductance. Since the conductance is determined by transmission via the generalized Landauer formula, it suffices to calculate the quantum transmission. As the electron energy is changed, the transmission of a quantum dot typically exhibits fluctuations. Through a systematic examination of patterns of the local density of states (LDS), we find a correlation between the fluctuations and the formation of scarring states inside the dot structure. These are also known as pointer states, the quantum states that remain robust when coupled to the external environment [19]. We find that, at the local maxima or local minima of the transmission curve, the LDS tends to concentrate on particular regions, such as those around periodic orbits when the dot structure is treated classically as an open billiard. Equivalently, the scarring states correspond to resonances in the transport dynamics. This is analogous to the one-dimensional transmission problem through a finite square potential well, where resonances can either enhance or suppress transmission, depending on the phase of the wavefunction. It should be noted that, in conventional semiconductor quantum dots, the conductance fluctuations have been found to be closely related to the appearance and disappearance of various scarring states, which transit to pointer states and to the quasi-classical region [20–22].

In section 2, we describe the non-equilibrium Green’s function formalism as applied to graphene quantum-dot structure. In section 3, we present results for transmission fluctuations and evidence of scarring and establish a correlation between them. A brief summary is given in section 4.

2. Non-equilibrium Green’s function formalism

Since GNRs and graphene quantum dots serve as the fundamental component of any graphene devices, we focus on calculating the conductance of these basic graphene structures, via the standard Landauer formula that relates the conductance $G(E_F)$ to the overall transmission $T_G(E_F)$ as [23]:

$$G(E_F) = \frac{2e^2}{h} T_G(E_F), \quad (1)$$

where

$$T_G(E_F) = \int T(E) \left(-\frac{\partial f}{\partial E} \right) dE,$$

$T(E)$ is the transmission of the device and $f(E) = 1/[1 + e^{(E-E_F)/kT}]$ is the Fermi distribution function. At low temperature, $-\partial f/\partial E \approx \delta(E - E_F)$, thus $T_G(E_F) = T(E_F)$ and $G(E_F) = (2e^2/h)T(E_F)$. To be concrete, we focus on the low-temperature conductance, or equivalently, the low-temperature transmission T .

We use the tight-binding framework and employ the NEGF formalism to calculate the transmission $T(E)$ for

graphene quantum dots [24, 25]. In general, the system can be divided into three parts: left lead, device, and right lead, where the left and the right leads are assumed to be semi-infinite and are not directly contacted (figure 1(a)). The device is chosen to include all the irregular parts so that the left and the right leads are uniform in the width. The Hamiltonian matrix can then be written as

$$H = \begin{pmatrix} H_L & H_{LD} & 0 \\ H_{DL} & H_D & H_{DR} \\ 0 & H_{RD} & H_R \end{pmatrix}, \quad (2)$$

whose elements are $-t$ for nearest-neighbor atoms and zero otherwise. In the Hamiltonian, H_D is a finite-size square matrix of dimension $N_D \times N_D$, N_D is the number of atoms in the device, and $H_{L,R}$ are the Hamiltonians of the left lead and right lead, respectively. The various couplings between the device and leads are given by the matrices H_{LD} , H_{DL} , H_{DR} , and H_{RD} . Using layer indices as subscripts, the Hamiltonian can be written in forms of layer Hamiltonians. For example, for the device shown in figure 1(b), we have

$$H_D = \begin{pmatrix} H_{11} & H_{12} & 0 & 0 & 0 \\ H_{21} & H_{22} & H_{23} & 0 & 0 \\ 0 & H_{32} & H_{33} & H_{34} & 0 \\ 0 & 0 & H_{43} & H_{44} & H_{45} \\ 0 & 0 & 0 & H_{54} & H_{55} \end{pmatrix},$$

where, for instance,

$$H_{11} = \begin{pmatrix} 0 & -t & 0 & 0 & 0 & 0 & 0 & 0 \\ -t & 0 & -t & 0 & 0 & 0 & 0 & 0 \\ 0 & -t & 0 & -t & 0 & 0 & 0 & 0 \\ 0 & 0 & -t & 0 & -t & 0 & 0 & 0 \\ 0 & 0 & 0 & -t & 0 & -t & 0 & 0 \\ 0 & 0 & 0 & 0 & -t & 0 & -t & 0 \\ 0 & 0 & 0 & 0 & 0 & -t & 0 & -t \\ 0 & 0 & 0 & 0 & 0 & 0 & -t & 0 \end{pmatrix},$$

is the Hamiltonian matrix for layer 1, whose size is $N_1 \times N_1 = 8 \times 8$, and

$$H_{12} = \begin{pmatrix} 0 & 0 & -t & 0 & 0 & 0 & 0 & 0 & 0 & 0 \\ 0 & 0 & 0 & 0 & 0 & 0 & 0 & 0 & 0 & 0 \\ 0 & 0 & 0 & 0 & 0 & 0 & 0 & 0 & 0 & 0 \\ 0 & 0 & 0 & -t & 0 & 0 & 0 & 0 & 0 & 0 \\ 0 & 0 & 0 & 0 & 0 & 0 & -t & 0 & 0 & 0 \\ 0 & 0 & 0 & 0 & 0 & 0 & 0 & 0 & 0 & 0 \\ 0 & 0 & 0 & 0 & 0 & 0 & 0 & 0 & 0 & 0 \\ 0 & 0 & 0 & 0 & 0 & 0 & 0 & -t & 0 & 0 \end{pmatrix},$$

is the coupling matrix from layer 2 to layer 1, which has a size of $N_1 \times N_2 = 8 \times 10$. Note that $H_{11} = H_{00} = H_{-1,-1} = \dots = H_{55} = H_{66} = \dots$, thus H_{11} is also the Hamiltonian for each layer of the leads. $t \approx 2.8$ eV is the nearest-neighbor hopping energy [2]. Note that in the calculation of transmission T , t is only a parameter in the energy, thus the results are independent of t if we normalize all energies by t . The finite-temperature conductance depends on t , though.

The NEGF $G(E)$ is defined by

$$(EI - H)G(E) = I, \quad (3)$$

where I is the identity matrix. Thus $G(E) = (EI - H)^{-1}$. Note that both G and H are for the whole system, which has

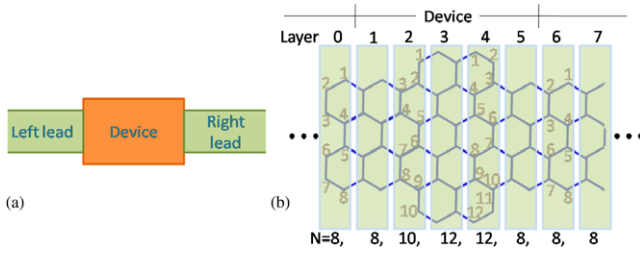


Figure 1. (a) Schematic illustration of a typical quantum dot. (b) Illustration of construction of various tight-binding Hamiltonians for calculating Green's function. The device consists of layer 1 to layer 5. The left lead is from layer $-\infty$ to layer 0; and the right lead is from layer 6 to layer ∞ . The numbers in the bottom of the figure indicate the number of atoms in each layer.

an infinite size. To calculate Green's function for the device, the effects of the leads can be treated as self-energies: Σ_L and Σ_R for the left and the right leads, respectively. Thus

$$G_D(E) = (EI - H_D - \Sigma_L - \Sigma_R)^{-1}, \quad (4)$$

where the self-energies are given by

$$\Sigma_L \equiv H_{DL}G_LH_{LD}, \quad \Sigma_R \equiv H_{DR}G_RH_{RD},$$

and $G_{L,R}$ are Green's functions for the left and the right leads.

Consider now the self-energy caused by the left lead (figure 2). Since only the nearest-neighbor interactions are considered, the coupling matrix H_{LD} , while having an infinite size, has only a finite number of non-zero elements that correspond to the coupling from the atoms on the left boundary of the device to the atoms on the surface of the left lead. The non-zero elements of the self-energy can be written as

$$\Sigma_l = V_0^\dagger G_l V_0,$$

where V_0 is the coupling from the left boundary of the device to the boundary of the left lead, and G_l is Green's function of the boundary atoms of the left lead. If the left boundary of the device has the same width as the left lead (which can always be realized by choosing the 'device' properly), then Σ_l satisfies the self-consistent Dyson equation:

$$\Sigma_l = V_0^\dagger (E - H_0 - \Sigma_l)^{-1} V_0, \quad (5)$$

where H_0 is the Hamiltonian of the left boundary atoms of the device, which is also the Hamiltonian for each layer of the left lead (figure 2). Similarly, the self-energy caused by the right lead satisfies

$$\Sigma_r = V_0(E - H_0 - \Sigma_r)^{-1} V_0^\dagger. \quad (6)$$

The above equations for self-energies can be solved numerically following a standard procedure [25]. Then the self-energy matrices $\Sigma_{L,R}$ can be obtained from an initial zero matrix of size $N_D \times N_D$ by filling the boundaries with $\Sigma_{l,r}$, after which the Green's function G_D can be calculated.

The coupling matrices $\Gamma_L(E)$ and $\Gamma_R(E)$ are the difference between the retarded and advanced self-energy caused by the coupling from the leads:

$$\Gamma_{L,R} = i(\Sigma_{L,R} - \Sigma_{L,R}^\dagger). \quad (7)$$

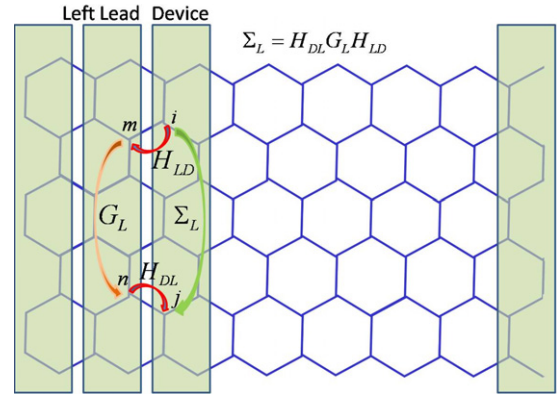


Figure 2. Schematic of calculation of self-energy Σ_L for the left lead.

Finally, the transmission T is given by

$$T(E) = \text{Tr}(\Gamma_L G_D \Gamma_R G_D^\dagger), \quad (8)$$

and the local density of states (LDS) for the device is

$$\rho = -\frac{1}{\pi} \text{Im}[\text{diag}(G_D)]. \quad (9)$$

3. Results

We start with an infinite GNR. Figure 3(b) shows the band structure for such a waveguide with zigzag boundaries, where $a_0 = \sqrt{3}a$ is the lattice constant and $a = 1.42 \text{ \AA}$ is the separation between the two neighboring carbon atoms in graphene. In each vertical layer there are $N = 24$ atoms. As the number of atoms becomes larger, the minimum energy values of the positive energy band approach zero, also do the maximum values of the negative energy band. In the limit $N \rightarrow \infty$, the two bands touch each other at the Dirac points, giving rise to the linear energy-momentum relation that is characteristic of relativistic motion. Figure 3(a) shows the transmission coefficient T of the same GNR as a function of the energy. Generally, for a given energy, the GNR may allow several propagating modes, corresponding to different k_x values, which have distinct wavefunctions along the y direction. These modes can be determined graphically by the crossing points of $E = \text{constant}$ with the various $E \sim k_x$ curves, as shown in figure 3(b). Each mode contributes unity to the transmission. Thus the total transmission is equal to the number of allowed propagating modes. Figure 3(c) shows the number of propagating modes n_E versus the energy E . It is exactly the same as the transmission shown in figure 3(a), validating our numerical algorithms.

Generally, when the shape of the device is non-uniform, the whole system including the leads is no longer invariant under translation in the x -direction, thus it does not have a unified dispersion relation, the $E \sim k$ curve. If the device is also a ribbon but with different width, then in each region (lead or device), the dispersion curve can be approximated by that for an infinite ribbon. Thus transport from one lead, say, left, through the device to the other lead is effectively a *quantum*

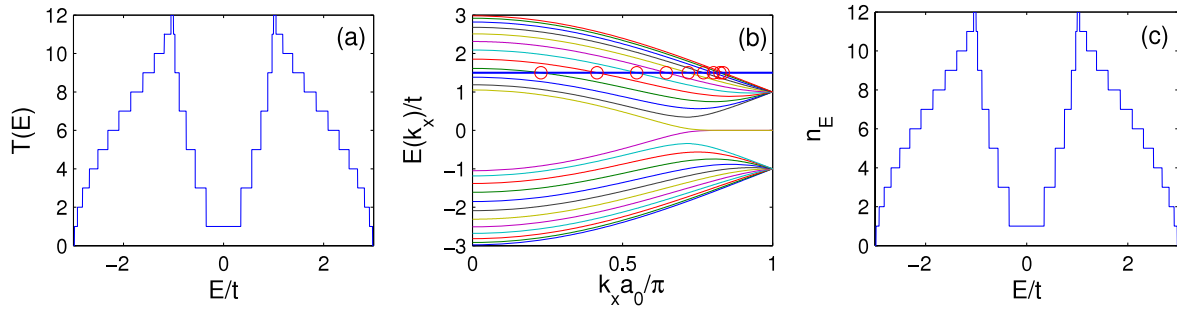


Figure 3. For an infinite zigzag GNR with 24 atoms in each layer, (a) transmission T versus energy E . (b) Band structure for $k_x > 0$. The circles indicate the allowed k_x values for a given energy, which correspond to the allowed propagating states. (c) The number of allowed propagating states n_E versus energy E .

scattering process [26, 27] from one allowed propagating state $k_{x,L}$, among many others, in the left lead to another $k_{x,D}$ in the device and then to $k_{x,R}$ state in the right lead, which is not necessarily the same as that in the left lead. The scattering is possible if the cross integrals of the transverse waves corresponding to $k_{x,L}$ and $k_{x,D}$, and also $k_{x,D}$ and $k_{x,R}$, are appreciable. As the energy varies, the allowed propagating wave numbers and their corresponding transverse waves all change, affecting the transmission. The transmission thus depends sensitively on the energy. Since one state in the lead can be scattered into several different allowed states in the device and vice versa, the transmission no longer takes on integer values, and the changes in transmission no longer occur in steps, but rather are represented by continuous variations.

Figure 4 shows a representative rectangular graphene quantum dot where the left and right leads are semi-infinite. Figure 5 shows the transmission versus energy for dots of different orientations and different sizes. The quantum dots for figures 5(a)–(c) have zigzag boundaries and the same width W_0 and W while their lengths are increased from (a) to (c). We observe that the transmission exhibits enhanced fluctuations as the dot length is increased. For all these three cases, since W is small, the transmission for low energies (contributed by the edge states) has a smaller degree of fluctuations, as compared to figure 5(d) where W is significantly larger. For case (a), the length of the quantum dot is also small, thus the transmission for high (or low) energy far from the Dirac point ($E/t \approx \pm 3$), corresponding to small wave vectors and long wavelengths, is the same as that for GNR, since effectively the transmitting waves cannot be scattered. The graphene dot for figure 5(d) has the same length as figure 5(b) but with a much larger width. As expected, this causes more disturbances to the edge states and thus exhibits larger fluctuations in the low energy region. Figures 5(e) and (f) show the transmission for graphene quantum dots with armchair boundaries for different sizes. Again, the fluctuation is enhanced as the dot becomes larger. Zooming into the fluctuation pattern, the scale of a peak/dip in terms of the energy is typically of the order of $0.0001t$ or even smaller. We have examined conductance fluctuations for several different dot shapes, including some shapes that have regular billiard behavior classically and a shape that is classically chaotic. For all the quantum dots studied we have found significant fluctuations in the transmission curve. For

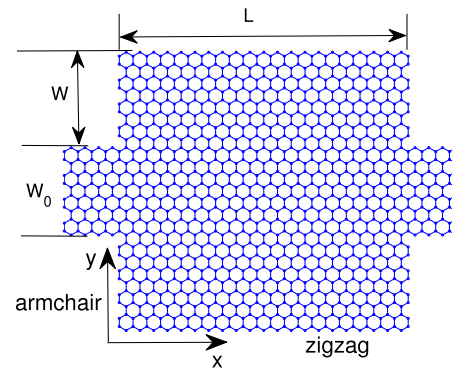


Figure 4. Rectangular graphene quantum dot with zigzag boundaries along x directions.

the region of small energy, it has been suggested that the zero-transmission resonance is due to the flux states [28]. In general, as we will demonstrate below, the fluctuations are caused by resonant transmission of electrons (or holes) in the graphene quantum dots.

We have systematically calculated LDS as the energy varies and found that generally, at a local peak or a local valley of the transmission, the corresponding LDS exhibits recognizable patterns. Near a peak or a valley, the pattern changes drastically as the energy varies. For energy in between local peaks and local valleys, the patterns become smeared and do not change appreciably with the energy. Figure 6 shows the transmission curve (a) and a series of LDS patterns ((b)–(f)) at different energies. Note that the color scale in different panels is different. In fact, for each pattern, we fix the light color (determined by a three-component vector) for the minimum value of LDS and the dark color for the maximum value and linearly map the LDS values (a one-dimensional interval) to the corresponding colors (a line segment in three-dimensional color parameter space). Since the atoms reside on a honeycomb lattice, we first sort the LDS value in ascending order, then plot at each site a solid circle with corresponding color code starting from those with small LDS values. When the energy varies, the wavefunction changes. At certain points, the wavefunction concentrates on small focused regions that contain classically periodic orbits, where electrons bounce back and forth along these orbits (see figures 6 and 7 for some

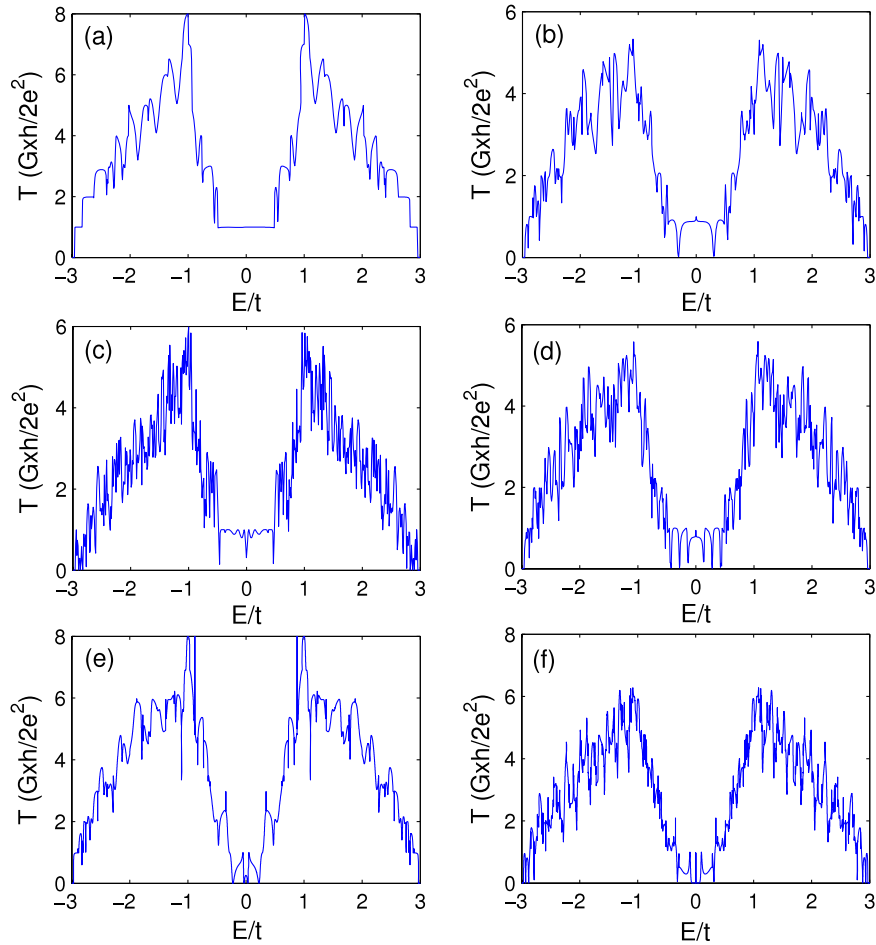


Figure 5. Transmission versus energy for different rectangular graphene quantum dots with zigzag boundaries (a)–(d) and armchair boundaries (e), (f). (a) $W = 4\sqrt{3}a_0$, $L = a_0$; (b) $W = 4\sqrt{3}a_0$, $L = 5a_0$; (c) $W = 4\sqrt{3}a_0$, $L = 20a_0$; (d) $W = 10\sqrt{3}a_0$, $L = 5a_0$. The width W_0 is given by $W_0 = 3\sqrt{3}a_0 + 2a_0/\sqrt{3} = 11a$, which is the same for all the quantum dots used in our computation. There are $N = 16$ atoms in each layer and a maximum of 8 transmission modes. (e) $W = 2a_0$, $L = 2\sqrt{3}a_0 - a = 5a$; (f) $W = 6a_0$, $L = 6\sqrt{3}a_0 - a = 17a$. $W_0 = 8a_0$, which supports a maximum of 8 transmission modes.

typical resonant orbits). This resonant behavior, which results in the presence of Fano resonances [29, 30] may enhance or suppress electron transmission through the quantum dot. From the figure we see that the local peaks or the local valleys in the transmission curve are associated with strong resonances. Comparing figures 6(b), (e) (valleys) and (d) (peak), we find that the resonance patterns corresponding to local valleys have small LDS values in the lead region. This can be seen intuitively since, as the electrons bounce back and forth in the graphene quantum dot following the concentration of the patterns, they are trapped within the dot, leading to a low transmission. However, exception can occur. As shown in figure 7, pattern (c) has small LDS values in the lead region, but its corresponding transmission is in fact a local maximum. When the patterns are well confined in the graphene dots, the electrons will traverse the orbits for a longer time before escaping. The longer the trapping time, the narrower the resonances are in energy, resulting in sharper peaks or dips in the transmission curve. This can be seen in figures 6(e) and 7(c), also in figures 8(c) and 9(b) for armchair boundaries.

To examine the dependence of LDS on lattice orientation, we have also calculated the LDS for rectangular graphene quantum dots with armchair boundaries along the x direction. The results are shown in figures 8 and 9 with resonant orbits indicated by the dashed lines. Comparing with the patterns for the quantum dots with zigzag boundaries, we observe similar patterns, e.g., those bouncing up and down in the y direction. A systematic check of the two configurations reveals that, although there are some common patterns, generally the patterns have different inclines for the two configurations. Specifically, the one with zigzag boundaries along x direction tends to have horizontal line shapes with relatively fewer vertical line shapes, while the other one has many resonant patterns with vertical trajectories but fewer horizontal line shapes. In contrary to the GaAs quantum dot where the electron motion is described by the Schrödinger equation with potential confinement in the dot boundaries [30], the electron motion in graphene quantum dots at low Fermi energy is described by Dirac equation. For a higher Fermi energy, the constant energy curves acquire a nontrivial trigonal warping distortion, thus the electron motion has to be analyzed

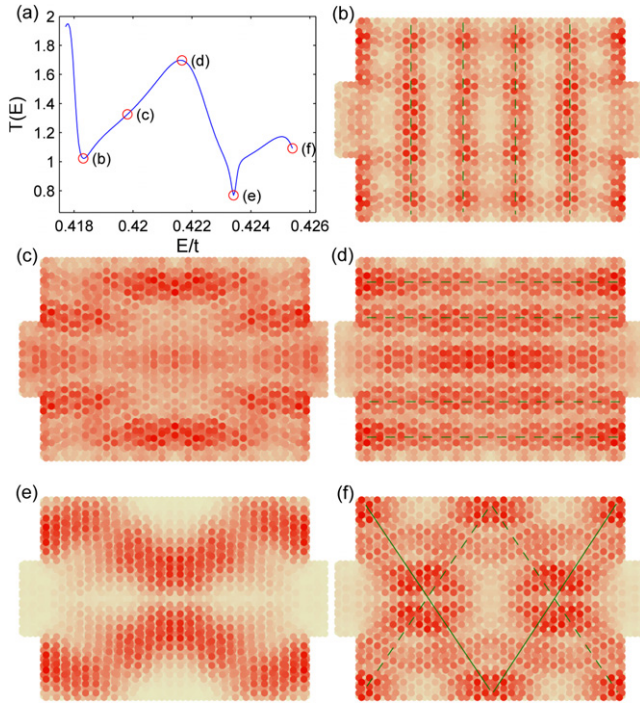


Figure 6. (a) Transmission versus energy. The circles indicate the energy and transmission values for the LDS patterns showing in (b)–(f). Dark (red) regions in the patterns correspond to higher local densities. The minimum and maximum LDS values of the patterns are $(5.29 \times 10^{-4}, 0.310)$, $(5.86 \times 10^{-4}, 0.072)$, $(9.60 \times 10^{-4}, 0.122)$, $(6.59 \times 10^{-4}, 1.198)$, $(3.42 \times 10^{-4}, 0.389)$ for (b)–(f), respectively. The size of the graphene dot is $W_0 = 8\sqrt{3}a_0 - a = 23a$, $W = 7\sqrt{3}a_0 = 21a$, $L = 50a_0$. The corresponding classical orbits, when appreciable, are plotted using solid or dashed line segments.

alternatively to include the distortions [31]. Since the electron motion and thus the pattern line shapes are affected by the $E-k$ functional form, which is basically characterized by the Dirac points for graphene, the difference in the tendency of pattern line directions is caused by the inequivalence of the configuration of the Dirac points for the two cases.

The observed resonant transmission is similar to the transmission through a finite one-dimensional quantum square well. Resonance causes fluctuation in the transmission curve, but depending on the phase of the wavefunctions, it may either enhance or suppress the transmission. For a two-dimensional quantum dot, the same scenario holds. For conventional semiconductor quantum dot of rectangular geometry, the transmission can be solved via the mode-matching technique [32]. For a graphene dot, the electron motion is governed by the Dirac equation, and under certain conditions the system can still be solved by mode-matching [33]. Note that some of the patterns are focused on classical periodic orbits. For irregular graphene quantum dots, e.g., the stadium shape, we have observed similar patterns. There is thus evidence of quantum scars in graphene quantum-dot structures. Since strong resonance of electrons in the quantum dot leads to local extreme values of transmission, it can be expected that larger quantum dots supporting more resonant states can exhibit stronger fluctuations in the transmission curve, as shown in figure 5. Again this result is

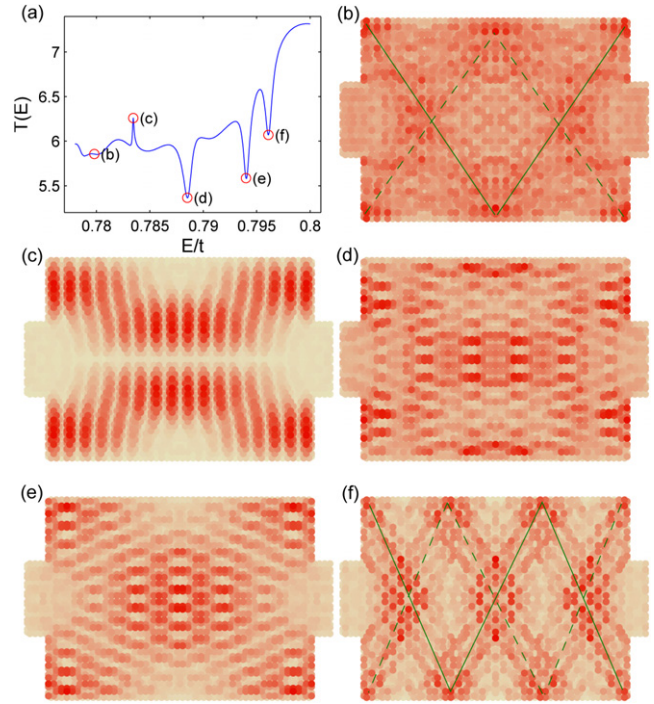


Figure 7. Resonant transmission patterns in a different energy level. The minimum and maximum LDS values of the patterns are $(1.45 \times 10^{-2}, 0.275)$, $(0.877 \times 10^{-2}, 1.419)$, $(1.52 \times 10^{-2}, 0.350)$, $(1.29 \times 10^{-2}, 0.534)$, $(0.720 \times 10^{-2}, 0.541)$ for (b)–(f), respectively. Other parameters are the same as in figure 6.

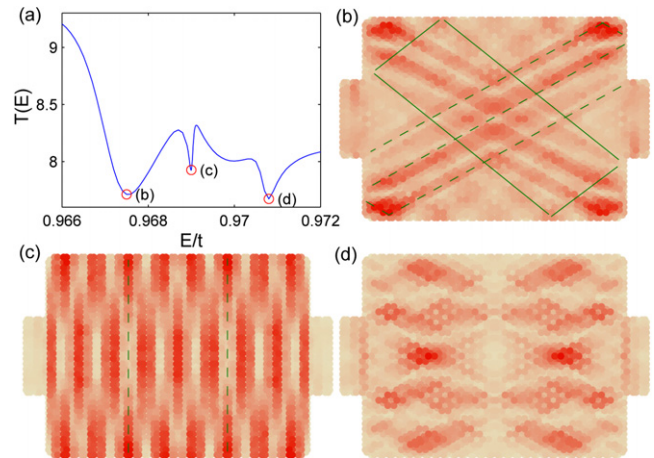


Figure 8. Resonant transmission patterns for a square graphene dot with armchair boundaries along x direction. The minimum and maximum LDS values of the patterns are $(1.26 \times 10^{-2}, 0.550)$, $(2.97 \times 10^{-2}, 1.842)$, $(1.73 \times 10^{-2}, 1.016)$ for (b)–(d), respectively. The size of the graphene dot is $W_0 = 14a_0$, $W = 12a_0$, $L = 29\sqrt{3}a_0 - a = 86a$. The corresponding classical orbits, when appreciable, are plotted using solid or dashed line segments.

analogous to that from the one-dimensional finite square well problem. For such a well with potential depth U_0 and length l , the transmission is maximum if $\sqrt{2m(E + U_0)}l/\hbar = n\pi$, where n is an integer, and minimum if $\sqrt{2m(E + U_0)}l/\hbar = (n + 1/2)\pi$. Thus when the length of the potential well l is increased, the energy difference between a local maximum

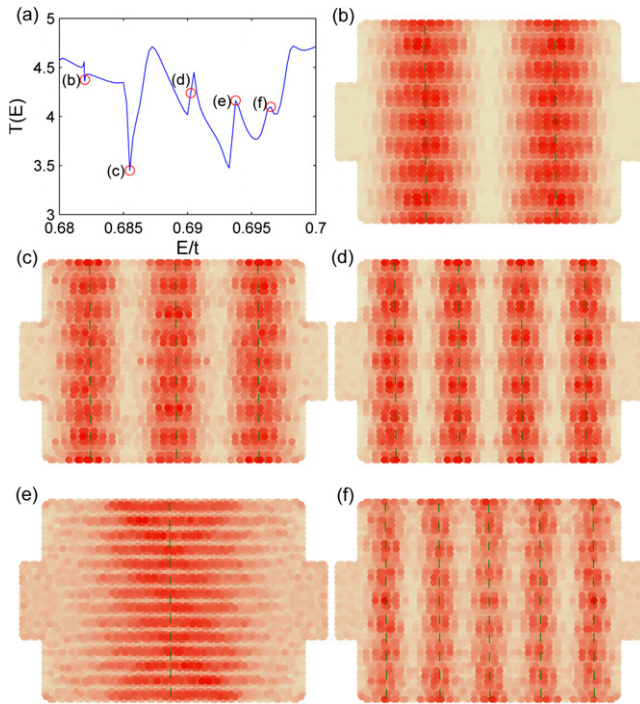


Figure 9. Resonant transmission patterns in a different energy level for the armchair graphene quantum dot. The minimum and maximum LDS values of the patterns are $(0.709 \times 10^{-2}, 1.160)$, $(1.01 \times 10^{-2}, 0.511)$, $(0.711 \times 10^{-2}, 0.519)$, $(0.759 \times 10^{-2}, 0.268)$, $(0.904 \times 10^{-2}, 0.371)$ for (b)–(f), respectively. Other parameters are the same as in figure 8.

and a neighboring minimum becomes smaller, leading to more significant fluctuations in the transmission curve.

4. Conclusion

We have studied the transmission of graphene rectangular quantum dots using the tight-binding approach and demonstrated transmission fluctuations with energy. The fluctuations are generally enhanced as the size of the dot is increased. There is a correlation between the fluctuations and the formation of scarring patterns in the LDS. In particular, near the local maxima or local minima of the transmission, scarring is relatively stronger, suggesting that the transmission fluctuations can be explained by the occurrence of various quantum resonances.

Acknowledgment

LH and YCL were supported by ONR under Grant No. N00014-08-1-0627.

References

[1] Wallace P R 1947 *Phys. Rev.* **71** 622
 [2] Castro Neto A H, Guinea F, Peres N M R, Novoselov K S and Geim A K 2009 *Rev. Mod. Phys.* **81** 109
 (Castro Neto A H, Guinea F, Peres N M R, Novoselov K S and Geim A K 2007 arXiv:0709.1163v2)

[3] Novoselov K S, Geim A K, Morozov S V, Jiang D, Katsnelson M I, Grigorieva I V, Dubonos S V and Firsov A A 2005 *Nature* **438** 197
 [4] Huard B, Sulpizio J A, Stander N, Todd K, Yang B and Goldhaber-Gordon D 2007 *Phys. Rev. Lett.* **98** 236803
 [5] Özyilmaz B, Jarillo-Herrero P, Efetov D, Abanin D A, Levitov L S and Kim P 2007 *Phys. Rev. Lett.* **99** 166804
 [6] Williams J R, DiCarlo L and Marcus C M 2007 *Science* **317** 638
 [7] Zhang L M and Fogler M M 2008 *Phys. Rev. Lett.* **100** 116804
 [8] Novoselov K S, Geim A K, Morozov S V, Jiang D, Zhang Y, Dubonos S V, Grigorieva I V and Firsov A A 2004 *Science* **306** 666
 [9] Berger C, Song Z, Li X, Wu X, Brown N, Naud C, Mayou D, Li T, Hass J, Marchenkov A N, Conrad E H, First P N and de Heer W A 2006 *Science* **26** 1191
 [10] Lemme M C, Echtermeyer T J, Baus M and Kurz H 2007 *IEEE Electron Device Lett.* **28** 282
 [11] Bolotin K I, Sikes K J, Jiang Z, Klima M, Fudenberg G, Hone J, Kim P and Stormer H L 2008 *Solid State Commun.* **146** 351
 Bolotin K I, Sikes K J, Hone J, Stormer H L and Kim P 2008 *Phys. Rev. Lett.* **101** 096802
 [12] Brey L and Fertig H A 2006 *Phys. Rev. B* **73** 235411
 Han M Y, Özyilmaz B, Zhang Y and Kim P 2007 *Phys. Rev. Lett.* **98** 206805
 Novikov D S 2007 *Phys. Rev. Lett.* **99** 056802
 Wassmann T, Seitsonen A P, Saitta A M, Lazzeri M and Mauri F 2008 *Phys. Rev. Lett.* **101** 096402
 Nakada K, Fujita M, Dresselhaus G and Dresselhaus M S 1996 *Phys. Rev. B* **54** 17954
 Muñoz-Rojas F, Fernández-Rossier J, Brey L and Palacios J J 2008 *Phys. Rev. B* **77** 045301
 [13] Ponomarenko L A, Schedin F, Katsnelson M I, Yang R, Hill E W, Novoselov K S and Geim A K 2008 *Science* **18** 356
 [14] Barone V, Hod O and Scuseria G E 2006 *Nano Lett.* **6** 2748
 [15] Han M Y, Özyilmaz B, Zhang Y and Kim P 2007 *Phys. Rev. Lett.* **98** 206805
 [16] Wang Z F, Shi Q W, Li Q, Wang X, Hou J G, Zheng H, Yao Y and Chen J 2007 *Appl. Phys. Lett.* **91** 053109
 [17] Barlas Y, Pereg-Barnea T, Polini M, Asgari R and MacDonald A H 2007 *Phys. Rev. Lett.* **98** 236601
 [18] Polini M, Tomadin A, Asgari R and MacDonald A H 2008 *Phys. Rev. B* **78** 115426
 [19] Zurek W H 2003 *Rev. Mod. Phys.* **75** 715
 [20] Ferry D K, Akis R and Bird J P 2004 *Phys. Rev. Lett.* **93** 026803
 [21] Brunner R, Meisels R, Kucher F, Akis R, Ferry D K and Bird J P 2007 *Phys. Rev. Lett.* **98** 204101
 [22] Brunner R, Akis R, Ferry D K, Kucher F and Meisels R 2007 *Phys. Rev. Lett.* **101** 024102
 [23] Landauer R 1970 *Phil. Mag.* **21** 863
 [24] Muñoz-Rojas F, Jacob D, Fernández-Rossier J and Palacios J J 2006 *Phys. Rev. B* **74** 195417
 [25] Li T C and Lu S-P 2008 *Phys. Rev. B* **77** 085408
 [26] Lai Y-C, Blümel R, Ott E and Grebogi C 1992 *Phys. Rev. Lett.* **68** 3491
 [27] de Moura A P S, Lai Y-C, Akis R, Bird J and Ferry D K 2002 *Phys. Rev. Lett.* **88** 236804
 Bird J P, Akis R, Ferry D K, de Moura A P S, Lai Y-C and Indlekofer K M 2003 *Rep. Prog. Phys.* **66** 583
 [28] Wakabayashi K and Sigrist M 2000 *Phys. Rev. Lett.* **84** 3390
 Wakabayashi K 2001 *Phys. Rev. B* **64** 125428
 [29] Fano U 1961 *Phys. Rev.* **124** 1866
 Göres J, Goldhaber-Gordon D, Heemeyer S, Kastner M A, Shtrikman H, Mahalu D and Meirav U 2000 *Phys. Rev. B* **62** 2188
 [30] Akis R, Bird J P, Vasileska D, Ferry D K, de Moura A P S and Lai Y-C 2003 *Electron Transport in Quantum Dots* ed J P Bird (Boston, MA: Kluwer Academic)

- [31] Saito R, Dresselhaus G and Dresselhaus M S 2000 *Phys. Rev. B* **61** 2981
Garcia-Pomar J L, Cortijo A and Nieto-Vesperinas M 2008
Phys. Rev. Lett. **100** 236801
- [32] Ferry D K and Goodnick S M 1997 *Transport in Nanostructures* (New York: Cambridge University Press)
- [33] Tworzydo J, Trauzettel B, Titov M, Rycerz A and Beenakker C W J 2006 *Phys. Rev. Lett.* **96** 246802